# Comparison of the *in vitro* and *in vivo* behavior of a series of NIR-II emitting aza-BODIPYs containing different water-solubilizing groups and their Trastuzumab Antibody Conjugates

Elisa Chazeau[a b c], Christol Fabre[d e], Malorie Privat[a], Amélie Godard[a], Cindy Racoeur[b c], Ewen Bodio[a], Benoit Busser[d e f], K. David Wegner[g], Lucie Sancey[d]*, Catherine Paul[b c]*, Christine Goze[a]*

[a] *ICMUB, UMR 6302 CNRS, Université de Bourgogne, 9 av. A. Savary, BP 47870, 21078 Dijon, France*

[b] *Laboratoire d'Immunologie et Immunothérapie des Cancers, EPHE, PSL Research University, 75000 Paris*

[c] *LIIC, EA7269, Université de Bourgogne, 21000 Dijon, France*

[d] *Université Grenoble Alpes, INSERM U 1209, CNRS UMR 5309, Institute for Advanced Biosciences, 38000 Grenoble, France*

[e] *Grenoble Alpes University Hospital (CHUGA), 38043 Grenoble, France*

[f] *Institut Universitaire de France (IUF), Paris, France*

[g] *Division Biophotonics, Federal Institute for Materials Research and Testing (BAM), 12489 Berlin, Germany*

**ABSTRACT**

The development of new fluorescent organic probes effective in the NIR-II region is currently a fast-growing field and represents a challenge in the domain of medical imaging. In this study, we have designed and synthesized an innovative series of aza-BODIPYs emitting in the NIR-II region. We have investigated the effect of differently water-solubilizing groups on the photophysical properties of the compounds, but also on their *in vitro* and *in vivo* performance, after bioconjugation to the antibody trastuzumab. Remarkably, we discovered that the most lipophilic compound unexpectedly displayed the most favorable *in vivo* properties after bioconjugation. This underscores the profound influence that the functionalization approach for the fluorophore can have on the efficiency of the resulting imaging agent.

## INTRODUCTION

Today, there is no doubt that fluorescence is one of the most popular imaging techniques from *in vitro* to clinical investigations, and in particular, for Fluorescence-Guided Surgery (FGS).[1,2] The expansion of diverse optical imaging applications has been paralleled by significant growth in the development of fluorescent probes, with a particular emphasis on organic fluorophores.[3] Among these fluorophores, cyanines have revolutionized the world of optical imaging, thanks to their brightness, making them the fluorophores of choice today, particularly for *in vivo* and clinical applications. However, other types of promising fluorophores are currently being developed, such as squaraines, xanthene derivatives, and BODIPYs or aza-BODIPYs.[4,5,6,7]

In particular, the aza-BODIPYs represent a very interesting family of dyes, since these molecules can emit in the NIR-I and/or NIR-II region, display a good brightness (which corresponds to the product of the quantum yield per the absorption coefficient), and more importantly are photochemically stable, especially compared to the cyanines.[8] Furthermore, these compounds are easily amenable to functionalization with various groups of interest, such as chelating agents for the development of bimodal probes or therapeutic compounds, enabling the creation of traceable therapeutic.[9,10]

However, one of the inherent disadvantages of aza-BODIPYs such as most of organic fluorophores is their lipophilic nature and the difficulty to render them water-soluble. Therefore, different strategies have been developed to increase the water-solubility of aza-BODIPYs. For example, introducing water-solubilizing groups on the core of the fluorophore or the replacement of the aromatic groups by non-aromatic groups.[11,12] A more effective approach involves substituting fluorine atoms with propargylamine groups. This substitution not only facilitates the crowding of the tetrahedral boron atom, thereby minimizing aggregation phenomena, but also enhances water solubility through the alkylation of the pendant $NMe_2$. Consequently, this process introduces additional positive charges to the fluorophore. This methodology was previously established for BODIPYs, and we have successfully adapted it to the aza-BODIPYs structure. This adaptation enables the desymmetrization of the molecule and facilitates the incorporation of diverse functionalities, including bioconjugatable groups.[13,14]

Implementing this strategy has resulted in the creation of water-soluble systems, termed Wazabys (where Wazabys denotes water-soluble aza-BODIPYs). These systems are amenable to bioconjugation with various vectors, including antibodies, as well as the incorporation of chelating agents, facilitating the development of multimodal probes or therapeutic complexes.[5]

We have also recently used this approach for aza-BODIPYs emitting in the NIR-II (named SWIR-Wazaby), compounds presenting no cytotoxicity.[15,16] Indeed, working in the NIR-II region – *i.e.*

between 1,000 and 1,700 nm – enables to greatly increase resolution compared to the NIR-I region, and thus to obtain better quality images.[17,18,19,20]

In addition to the recent publication of numerous preclinical studies, the substantial advantages of operating within the NIR-II region, as opposed to NIR-I, have recently been affirmed in a clinical context through the initiation of the first human study on fluorescence-guided surgery (FGS).[21]

The distinctive attributes of fluorophores designed for NIR-II imaging, encompassing brightness, stability, and hydrophobicity, exert a significant impact on their pharmacokinetic properties, thereby influencing their overall imaging efficiency. However, an aspect that has received limited exploration, particularly in the realm of NIR-II-emitting BODIPYs, pertains to the influence of the chosen water-solubilizing group on the fluorophore. These water-solubilizing groups may carry different charges, thereby exerting a substantial influence on the behavior of the fluorophore. Furthermore, even post-bioconjugation to a biological vector such as a peptide or antibody, the properties of the resultant imaging agents can undergo alterations contingent on the specific water-solubilizing groups employed, as previously demonstrated with cyanine dyes.[22] That is why, in this study, we wanted to investigate the influence of the overall charge on the SWIR-Wazaby compounds.

A first bioconjugatable SWIR-Wazaby has been developed by our group.[11] In this work, we changed the structure design in order to decrease the lipophilic character of the probe, and we also varied the solubilizing moieties in order to study their influence on the *in vitro* and *in vivo* properties of the resulting dyes.

We also worked on the bioconjugation of the series of fluorophores we developed. We decided to investigate a transglutaminase mediated bioconjugation,[23,24] which enables to work on fluorophores carrying $NH_2$ groups, thus avoiding the introduction of hydrophobic bioconjugatable moieties.

This work entails the synthesis of three target molecules, accompanied by a comprehensive examination of their photophysical and biological characteristics through in vitro and in vivo studies. A specific emphasis is placed on the potential influence of the water-solubilizing group on various properties, including photochemical attributes, lipophilic character, bioconjugation feasibility, and in vitro/vivo behavior of the resulting fluorophores. The objective is to identify the most promising compound for imaging applications.

## RESULTS AND DISCUSSSION

### Synthesis

The three targeted structures are represented in Figure 1. More precisely, we aimed at functionalizing the $NMe_2$ groupments by introducing on one hand a polyethylene glycol spacer directly tethered on the $NMe_2$ group, and on the other side two water-solubilizing groups, *i.e.,* an ammonium group or a sulfobetaine group (giving a zwitterionic moiety). We also studied the structure bearing the neutral $NMe_2$ group (*i.e.,* without the addition of any solubilizing group), which is expected to give the more lipophilic structure.

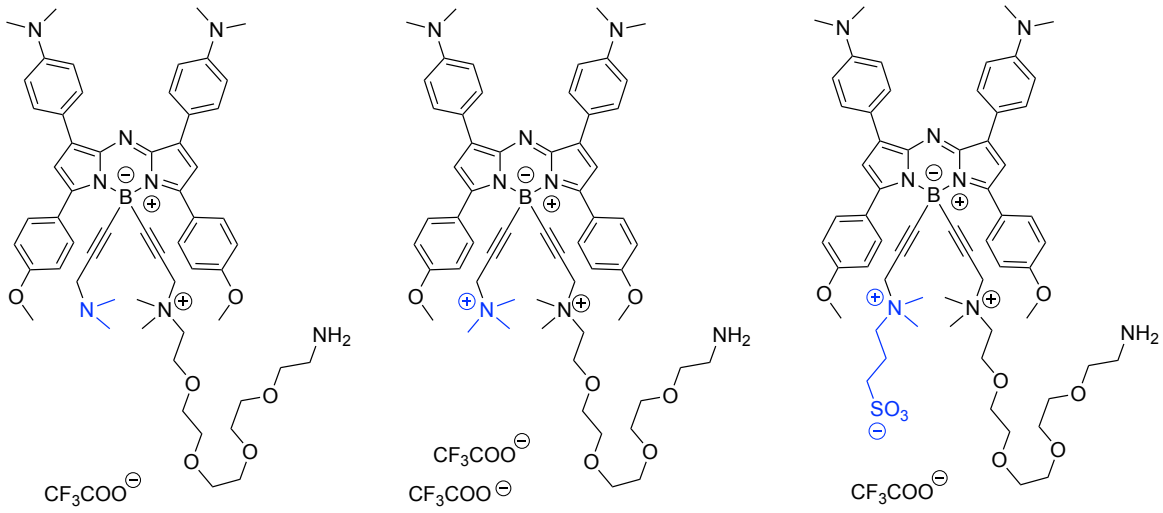

**($NMe_2$) AzaNIR II** **($NMe_3^+$) AzaNIR II** **($SO_3^-$) AzaNIR II**

***Figure 1****: targeted structures. Left: without any additional group on the second $NMe_2$ moiety. Middle: functionalized with an ammonium group. Right: functionalized with a sulfobetain groupment.*

The precursor **5** was synthesized *via* an adapted procedure from the synthetic pathway we described before for this compound (see Supporting information for synthetic details, Scheme S1).[8]

The mono-functionalization of one of the propargylamine groups on **5** can be performed either by opening the propanesultone at reflux, which led to the formation of pure **6** after purification, or **7** by using a nucleophilic substitution with the *N*-Boc-$PEG_4$-bromide leading to product **7** (Scheme 1). While the second reaction is more difficult to control (resulting in a mixture of starting material **5**, the mono and the di-substituted compounds), the opening of the propanesultone can be well controlled. After refluxing for 18 h in the presence of 5 equivalents of $NaHCO_3$, the desired mono-functionalized **6** product was obtained in 60% yield (since the formation of the bis substituted appears only after 48 h). Then, nucleophilic substitution with *N*-Boc-$PEG_4$-bromide followed by deprotection of the primary amine group gave compound **($SO_3^-$) AzaNIR II** in 80% yield (Scheme 1). It should be noted that this approach is very interesting as it opens the door to the introduction of numerous groups of interest on the propanesultone-monosubstituted compound.

In parallel, **($NMe_2$) AzaNIR II** was obtained after deprotection of the Boc group on **7**, and **($NMe_3^+$) AzaNIR II** could be synthesized after addition of an excess of $CH_3I$ on **7**, followed by direct deprotection of primary amine group (Scheme 1).

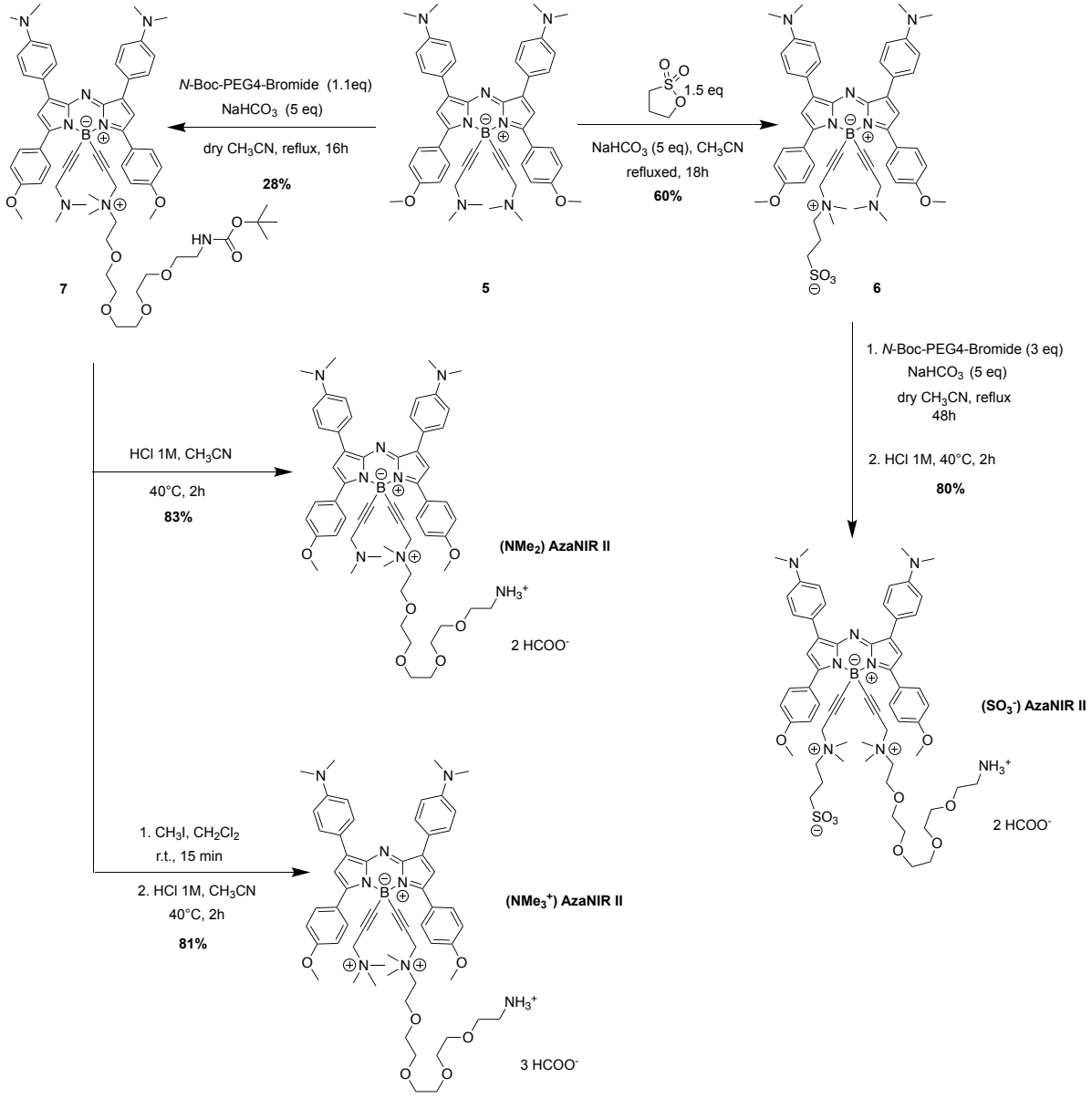


***Scheme 1**: Synthetic pathway for the targeted compounds **($NMe_2$) AzaNIR II, ($NMe_3^+$) AzaNIR II,** and **($SO_3^-$) AzaNIR II**.*

All the compounds have been characterized by $^1H$, $^{13}C$, $^{11}B$ NMR, as well as by High Resolution Mass Spectrometry (HR-MS). Additionally, there are all completely water-soluble.

The lipophilic character of the different compounds was then investigated (Table 1) with a reported HPLC method.[25] First of all, it should be noted that whatever the charge and groups on the fluorophore

were, they remained relatively lipophilic. Moreover, it is clear that two charges on the aza-BODIPYs are needed to drastically diminish this lipophilic character. The most lipophilic compound remains compound **(NMe$_2$) AzaNIR II**, for which only one of the two amines is functionalized.

Additionally, by comparing **(NMe$_3^+$) AzaNIR II** and **(SO$_3^-$) AzaNIR II**, we can observe that **(NMe$_3^+$) AzaNIR II** carrying the ammonium group is the most hydrophilic compound (log P = 1.90), and that compound **(SO$_3^-$) AzaNIR II** is more lipophilic despite the presence of sulfobetaine (log P = 2.34).

**Table 1**: Log P of the different compounds.

| Compounds | logP |
|---|---|
| **(NMe$_2$) AzaNIR II** | 3.76 |
| **(NMe$_3^+$) AzaNIR II** | 1.90 |
| **(SO$_3^-$) AzaNIR II** | 2.34 |

**Photophysical studies:**

The photophysical properties of the three compounds **(NMe$_2$) AzaNIR II**, **(NMe$_3^+$) AzaNIR II**, and **(SO$_3^-$) AzaNIR II**, as well as the mono sulfonated precursor **6** were studied in DMSO, PBS and PBS+10% FBS. The photophysical data in DMSO and PBS +10%FBS are summarized in Table 2. As previously observed, none of the compounds is fluorescent in PBS, very probably due to aggregation phenomena regarding the shape of the absorption (ESI section, Figure S11).

**Table 2**: Photophysical studies of the different compounds measured at 298K.

| Compound | Solvent | $\lambda_{abs}$[a] (nm) | $\lambda_{em}$ (nm) | $\varepsilon$ ($M^{-1}.cm^{-1}$) | $\Phi$ (%)[b] | Brightness (= $\varepsilon$*$\Phi$) |
|---|---|---|---|---|---|---|
| **6** | DMSO | 768 | 977 | 31,000 | 0.7 | 217 |
| **(NMe$_2$) AzaNIR II** | DMSO | 777 | 982 | 28,000 | 0.6 | 168 |
| **(NMe$_3^+$) AzaNIR II** | DMSO | 777 | 982 | 16,000 | 0.5 | 80 |
| **(SO$_3^-$) AzaNIR II** | DMSO | 777 | 980 | 27,000 | 0.6 | 162 |
| **6** | PBS+10%FBS | 738 | 820 | 40,100 | 4 | 1604 |
| **(NMe$_2$) AzaNIR II** | PBS+10%FBS | 738 | 826 | 34,000 | 3.3 | 1122 |
| **(NMe$_3^+$) AzaNIR II** | PBS+10%FBS | 747 | 820 | 18,000 | 2 | 360 |
| **(SO$_3^-$) AzaNIR II** | PBS+10%FBS | 747 | 822 | 22,000 | 1.8 | 396 |

[a] $\lambda_{abs}$ for the lowest energy absorption band; [b] relative measurements ($\Phi$) were performed using IR125 in ethanol as reference ($\lambda_{exc}$ = 770 nm).

The absorption and emission wavelengths of the various structures exhibit minimal differences. In DMSO, all structures display a distinctive "two bands" absorption profile characteristic of the aza-BODIPY core, featuring a lower energy absorption band around 777 nm. Notably, a significant variation is evident in the absorption coefficient of the compounds. While **6**, **($NMe_2$) AzaNIR II**, and **($SO_3^-$) AzaNIR II** show comparable ε values (with a maximum of 30,000 $M^{-1}$. $cm^{-1}$ for **6**), the absorption of **($NMe_3^+$) AzaNIR II** is less intense (ε = 16,000 $M^{-1}.cm^{-1}$). Conversely, there is no discernible distinction in the emission of the different structures, with equivalent quantum yields observed for all.

In the presence of 10% serum, both absorption and emission wavelengths undergo a pronounced blue shift in comparison to DMSO, with $\lambda_{abs}$ and $\lambda_{em}$ measuring 747 nm and 820 nm, respectively (Figure 2). This substantial shift, exceeding 100 nm, has been previously observed in studies focusing on aza-BODIPYs structures. It underscores the significance of exploring photophysical properties beyond traditional solvents like DMSO and delving into biological media to gain a more comprehensive understanding of the behavior of these fluorophores *in vivo*. The observed shift is likely attributable to non-covalent binding interactions between the dyes and plasma proteins.

The impact of serum on the behavior of fluorophores has been previously noted and can be elucidated through the interactions of these molecules with plasma proteins, particularly low-density lipoproteins (LDL) in the case of aza-BODIPYs. Similar effects have been investigated in the context of other near-infrared II (NIR-II) emitting fluorophores, leading to an enhancement of fluorescence. This phenomenon is dependent on the functionalization of the fluorophore, allowing for the preferential formation of a molecule-protein complex. Moreover, the absorption coefficient of the two compounds with a single functionalized $NMe_2$ group (**6** and (**$NMe_2$) AzaNIR II**) is nearly double compared to the compound where both $NMe_2$ groups are alkylated. This trend is also reflected in the fluorescence quantum yield, with values of 4 and 3.3 % for **6** and (**$NMe_2$) AzaNIR II**, respectively, in contrast to 1.8 and 2 % for **($SO_3^-$) AzaNIR II** and **($NMe_3^+$) AzaNIR II**. Overall, the emission is significantly more intense in the presence of serum compared to DMSO. However, the resulting brightness is more favorable for structures bearing only one functionalized $NMe_2$ group.

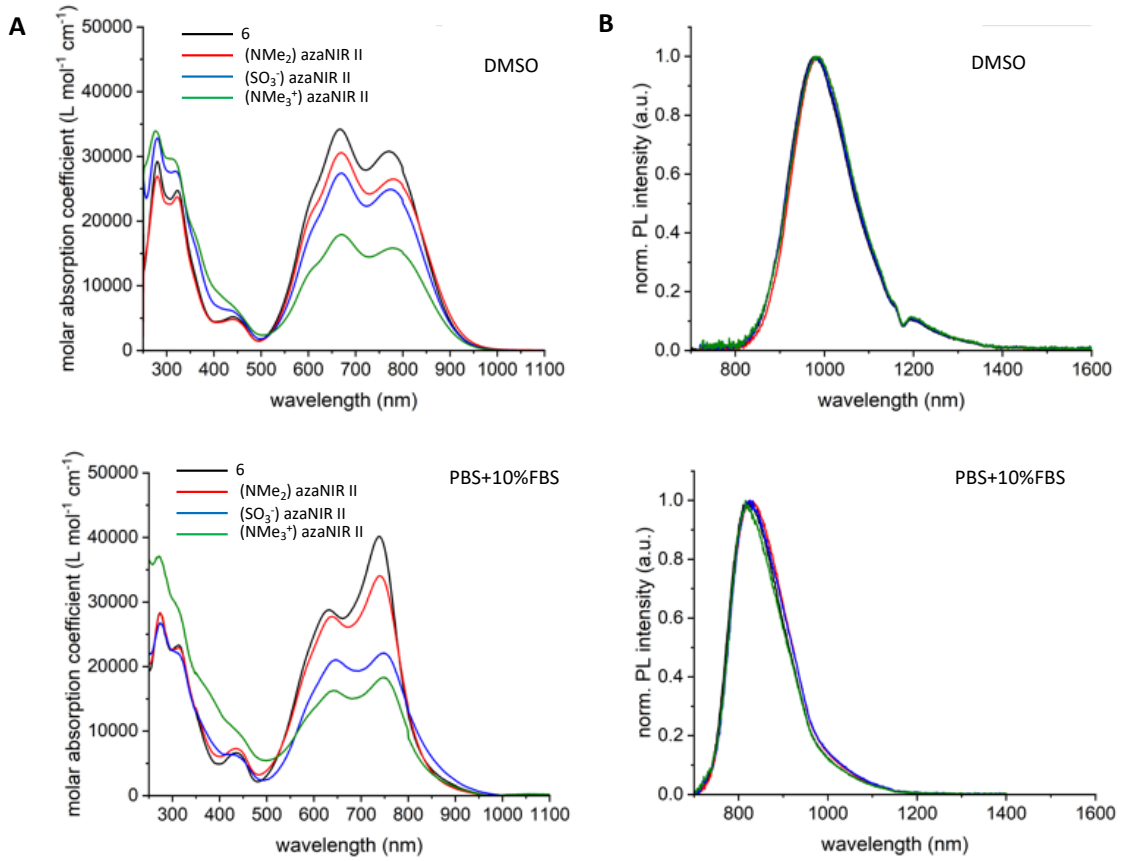


***Figure 2**: Absorption (A) and emission (B) of the different fluorophores in DMSO (top) and PBS+10%FBS (bottom) measured at 298K.*

**Bioconjugation**

To target specifically cancer cells, the three NIR-II probes were bioconjugated site-specifically to the FDA approved anti-HER2 monoclonal antibody (mAb) namely, trastuzumab, and on which we previously bioconjugated our aza-BODIPYs probes.[16] Indeed, the advantage of a site-specific conjugation in regard to random conjugation has been clearly proven.[26] In particular, for optical imaging using aza-BODIPYs fluorophores, we previously observed that an improved *in vivo* behavior of the conjugates has been reported when the fluorophore was grafted site-specifically to the biovector.[27,28] Therefore, it was crucial for us to conjugate the fluorophores in a site-specific manner.

Until now, we have always performed site-specific bioconjugation on glycan-modified antibodies using the Genovis kit (Glyclick).[29] In this work, we explored a site-specific bioconjugation strategy *via* the action of transglutaminase.[23] This enzymatic conjugation affords homogenous conjugates with a controlled DOL (degree of labeling) of 2 through the action of microbial transglutaminase (MTGase), which catalyzes transpeptidation between a primary amine of the side chain of glutamine of a deglycosylated IgG1 (Figure 3).

The removal of *N*-glycan chains from the mAb is required prior to mAb–linker conjugation. This withdrawal of the glycan chains allowed the MTGase to catalyze the reaction between the NIR-II probes and the glutamine 298 localized on the heavy chain of the antibody.

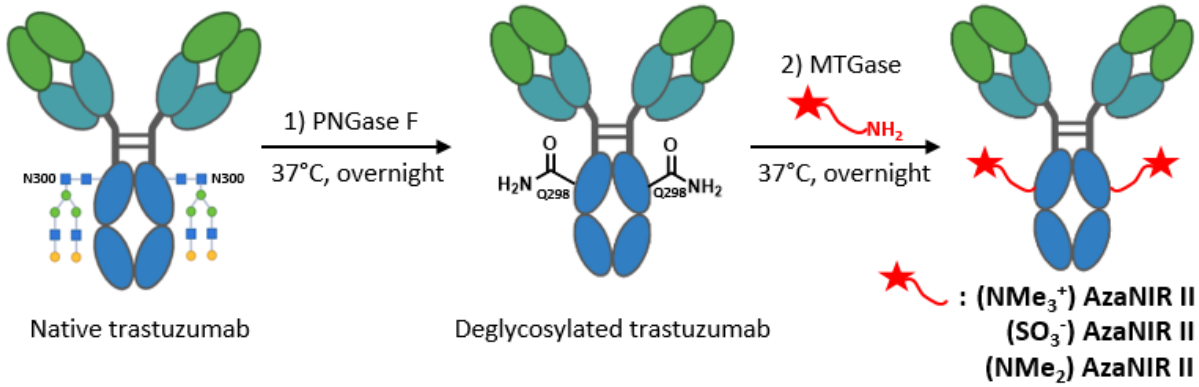


***Figure 3:*** *Synthesis of the three bioconjugates (1) PNGase F (500 U per mg of mAb), PBS pH 7.4, 37°C, overnight (2) AzaNIR II probes (20 eq), MTGase (3 U per mg of mAb), PBS pH 7.4, 37°C, overnight.*

The transglutaminase bioconjugation possesses many advantages (less expensive, two-step conjugation) compared to the method based on enzymatic glycan remodeling. However, one drawback for this approach is the apparent requirement of a high number of fluorophores' equivalents (which can increase up to 80 equivalents) to perform the enzymatic conjugation according to literature.[30] Even though the addition of a PEG moiety and water-solubilizing groups greatly improves the overall solubility of the probes, the aza-BODIPYs in general remain quite lipophilic structures, which could lead to tricky purification steps after the bioconjugation, and which needs a large excess of aza-BODIPYs. Moreover, the acceptance of MTGase toward larger amine-functionalized chemical entities is unpredictable.[31]

Therefore, in order to apply this method of bioconjugation to the new aza-BODIPYs fluorophores, we performed several optimizations. In particular, after the deglycosylation of trastuzumab by the action of PNGase F, the number of fluorophores equivalents incubated in presence of MTGase was easily reduced to 20 equivalents, without affecting the resulting conjugation. Finally, the site-specific bioconjugation allowed us to obtain a DOL around 2 for each probe, according to mass spectrometry analyses, with an average yield of 60% in two steps. We were therefore pleased to observe that, in this case, the action of MTGase was not negatively impacted by relatively large substrates, such as the AzaNIR II probes (Table 3 and Figure S13 in the ESI section). The different masses of deglycosylated antibody engaged in the reaction, the corresponding DOL and bioconjugation yields after purification are listed in the Table 3.

**Table 3**: Results of the bioconjugation reactions for each NIR II probes

| Bioconjugates | Mass of engaged deglycosylated trastuzumab | DOL | Bioconjugation Yield |
|---|---|---|---|
| **Trastu-($NMe_2$) AzaNIR II** | 1.5 mg | 1.9 | 76 % |
| **Trastu-($NMe_3^+$) AzaNIR II** | 1.5 mg | 1.8 | 56 % |
| **Trastu-($SO_3^-$) AzaNIR II** | 1.5 mg | 1.9 | 70 % |

The site-specific nature of the bioconjugation reaction was then verified *via* SDS-PAGE revealed by a stain-free imaging technology (Figure 4a) or by fluorescence with an IRdye800 filter on a ChemiDoc MP imaging system (Bio-Rad, Figure 4b). The denaturing electrophoresis gel experiment displayed a clear upward shift in the molecular weight of the heavy chain (named HC in the Figure 4) following the ligation of the probes to the deglycosylated trastuzumab. In contrast, no shift was observed for the light chain, demonstrating the site-specific character of the conjugation. In addition, the fluorescence was only located on the heavy chain for each NIR-II probes and no fluorescence was observed on the light chain.

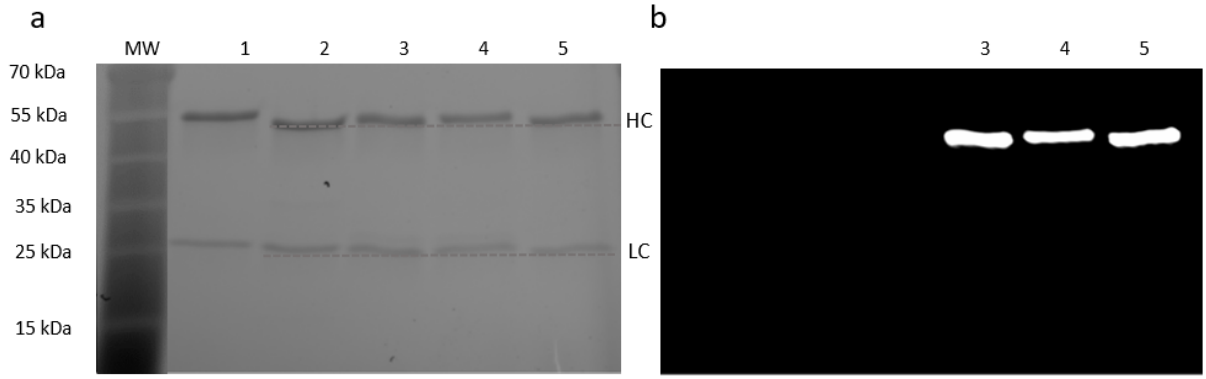


***Figure 4:*** *Denaturing polyacrylamide gel electrophoresis revealed by (a) stain-free imaging technology or by (b) fluorescence with an IRdye800 filter (excitation laser Epi-near IR, 755-777 nm, emission filter Near IR: 813-860 nm) on a ChemiDoc MP imaging system (Bio-Rad)) of (1) native trastuzumab, (2) Deglycosylated trastuzumab, (3)* ***Trastu-($NMe_2$) AzaNIR II****, (4)* ***Trastu-($NMe_3^+$) AzaNIR II*** *and (5)* ***Trastu-($SO_3^-$) AzaNIR II****, demonstrating the site-specific conjugation on the heavy chain. HC, heavy chains; LC, light chains.*

The affinity of the resulting bioconjugates toward HER-2 was assessed by biolayer interferometry (BLI). The addition of NIRII fluorophores to trastuzumab did not affect significantly the binding capacity of

the antibody for its target (Table 4, and Figure S14 ESI). Indeed, the calculated $K_D$ for each bioconjugate was in the same molar range than the one determined for native and deglycosylated trastuzumab (Table 4), even if **($SO_3^-$) AzaNIR II** seems to have a slightly lesser impact than the other two probes.

***Table 4:*** *Calculated $K_D$ for each species by BLI.*

| | $K_D$ |
|---|---|
| trastuzumab | $2.8.\ 10^{-10} \pm 3.\ 10^{-12}$ M |
| Deglycosylated trastuzumab | $4.3.\ 10^{-10} \pm 3.\ 10^{-12}$ M |
| **Trastu-($NMe_2$) AzaNIR II** | $5.3.\ 10^{-10} \pm 8.\ 10^{-12}$ M |
| **Trastu-($NMe_3^+$) AzaNIR II** | $5.4.\ 10^{-10} \pm 9.\ 10^{-12}$ M |
| **Trastu-($SO_3^-$) AzaNIR II** | $3.4.\ 10^{-10} \pm 9.\ 10^{-12}$ M |

Finally, the tendency to form aggregates of each conjugate was evaluated with size-exclusion chromatography (SEC) analysis. The proportion of aggregates was compared according to the grafting probes (Table S1 in the ESI section). **Trastu-($NMe_3^+$) AzaNIR II** and **Trastu-($SO_3^-$) AzaNIR II** were not prone to aggregation with very low aggregation rate (<1%). Nevertheless, for **Trastu-(NMe2) AzaNIR II**, the proportion of aggregates was higher than the two other bioconjugates (around 6% after the bioconjugation step). **Trastu-(NMe2) AzaNIR II** presents therefore a higher propensity for aggregation. This result is in agreement with the more lipophilic character of the **($NMe_2$) AzaNIR II** probe.

***In vitro* studies**

The different *in vitro* studies were performed on HER-2 expressing cells SKOV-3, and HER-2 non expressing cells OVCAR-3 (both are human ovarian cancer cell lines).

Cells were incubated with the different compounds, alone or conjugated to trastuzumab. While the charged compounds **($NMe_3^+$) AzaNIR II** and **($SO_3^-$) AzaNIR II** were observed on the membrane and in the cytoplasm of both cell types, the more lipophilic **($NMe_2$) AzaNIR II** was mainly detected on the cell membranes (Figure 5). Additionally, the charged compounds **($NMe_3^+$) AzaNIR II** and **($SO_3^-$) AzaNIR II** accumulated more than **($NMe_2$) AzaNIR II** in cells. As expected, the conjugated compounds were observed at the cell surface of the HER2-positive cells SKOV-3, after 1 h of incubation at 4 °C. The bioconjugated compounds were not detected at the surface of HER2-negative cells OVCAR-3.

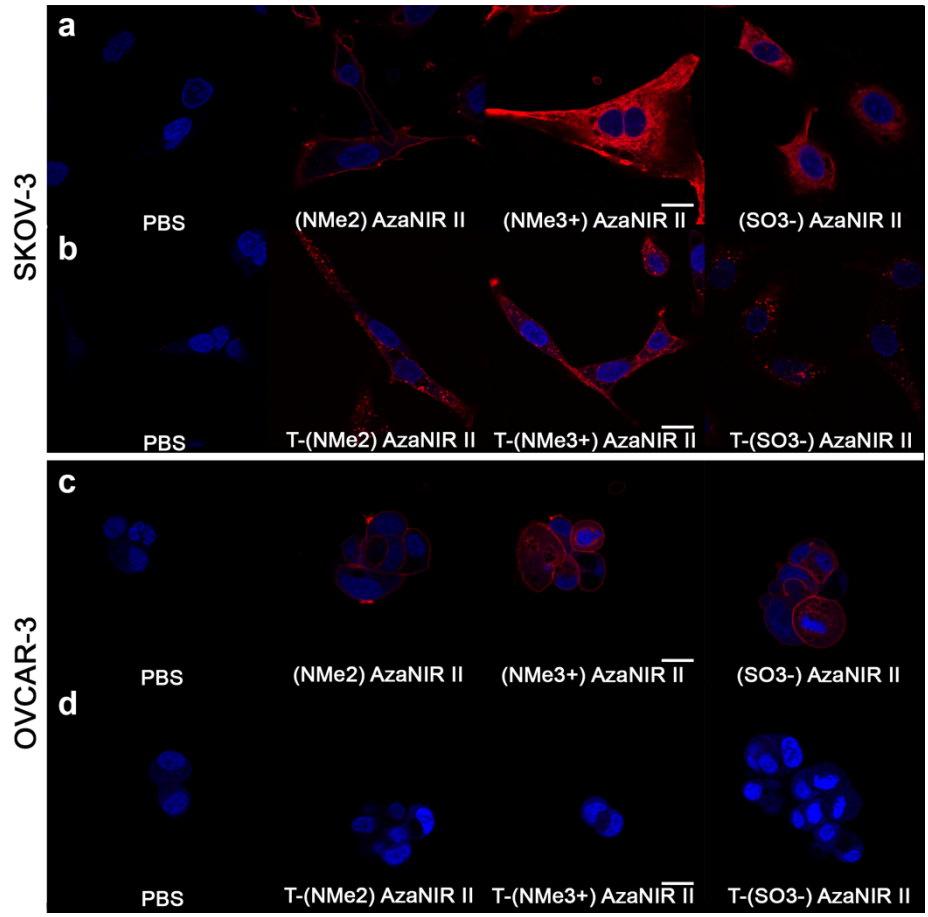


***Figure 5:*** *Confocal images of SKOV-3 (a,b) and OVCAR-3 (c,d) after 1 h of incubation at 4°C with PBS,* ***(NMe₂) AzaNIR II, (NMe₃⁺) AzaNIR II*** *and* ***(SO₃⁻) AzaNIR II*** *alone (a,c, 5 µg/mL), or conjugated with trastuzumab (T) antibody (b,d, 1 µg/mL) (red color). Excitation 633 nm; Emission >650 nm. Nucleus are stained in blue with Hoechst 33342. Scale bar: 10 µm.*

Such observations were confirmed using FACS analysis. After 2 h of incubation at 37 °C, the fluorophores were detected in both cell types, while only cell-expressing HER-2 were labeled with the trastuzumab-conjugated fluorophores. At 37 °C, the cell internalization of the different fluorophores alone was almost similar for the two cell lines (see ESI section Figure S16 and Table S2).

### *In vivo* studies and *ex vivo* biodistribution

The distribution of the compounds was then investigated *in vivo*, in mice bearing subcutaneous SKOV-3 tumors to observe the impact of the charge on the behavior of the compounds using epifluorescence NIR-II imaging (Figure 6a). To this end, all the non bioconjugated compounds were diluted in DMSO and then in PBS, with a final concentration < 2% of DMSO, *i.e.*, 5 times less than the maximum recommended dose of 10% v/v.

Mice were imaged at different time-points from 5 h to 48 h. The distribution was confirmed *ex-vivo* with a list of 13 organs and tumor (Figure 6b, and Figure S17). The two charged fluorophores significantly accumulated in the liver, adrenal gland and spleen as compared to **(NMe$_2$) AzaNIR II** ($p < 0.05$, one-way ANOVA), 48 h after intravenous administration. For all the three fluorophores, the tumors were identified with contrasts almost comparable from 5 to 48 h post injection (see Supplementary Table S3). At this late time-point, the *ex vivo* tumor-to-muscle ratios were higher than 3 for all the conditions, but the tumor-to-ovary ratios were < 1 (Figure 6c) and tumor-to-skin ratios were ~ 1.

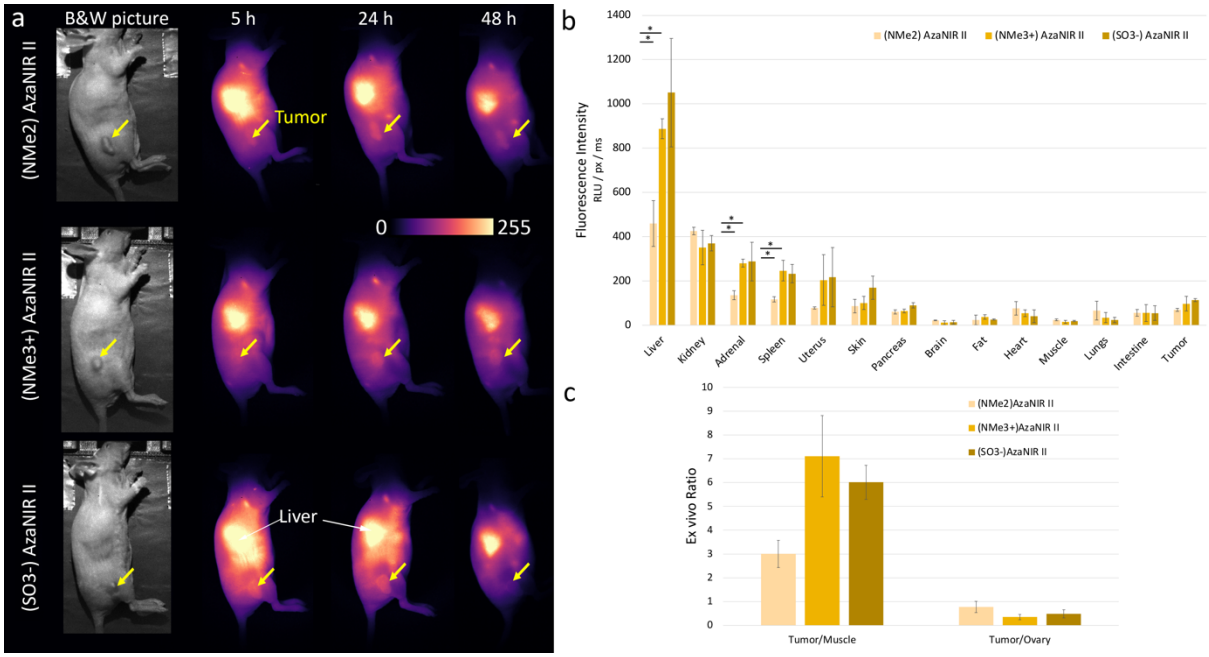


***Figure 6**: In vivo behavior of the different fluorophores. (a) Representative NIR-II images obtained with a Princeton camera of mice bearing subcutaneous SKOV-3 tumors on their right flank at different times elapsed after administration of 40 nmol non-coupled fluorophores. Tumors are evidenced with a yellow arrow, and livers are evidenced with white arrows. Color scale was standardized for all the captions. (b) Ex vivo distribution of **(NMe$_2$) AzaNIR II** (light yellow), **(NMe$_3^+$) AzaNIR II** (yellow), and **(SO$_3^-$) AzaNIR II** (dark yellow) at 48 hours. * indicates a significant difference between conditions, with $p < 0.05$. (c) Related tumor-to-muscle and tumor-to-ovary ratios, from (b) data. N = 3 /condition.*

To increase tumor accumulation, the fluorophores were coupled to trastuzumab and injected intravenously to mice-bearing SKOV-3 tumors, expressing the targeted HER-2 receptor. The injected dose was adjusted to the amount of antibody, strongly decreasing the number of fluorophores as compared to the previous experiments (1.4 nmol/mouse *versus* 40 nmol/mouse, respectively, Figure 7). In general, trastuzumab and antibodies circulate for prolonged time as compared to small

molecules; therefore, the images and the distributions were performed until 48 h and 6 days post injection for the three coupled-fluorophores. As expected for antibodies, the three coupled-compounds were mainly eliminated through the hepatobiliary route, and were also found in the kidneys, which can express HER-2 receptor in the tubules and the collecting ducts. The other organs did not accumulate specifically the AzaNIR II-trastuzumab compounds (supplementary Figure S17).[32]

Specific tumor targeting was obtained for the three compounds with an increase of the fluorescence with time and a favorable tumor-to-surrounding tissue contrast allowing the delineation of the tumors at 48 h and 6 days post-injection (see also supplementary Table S3). The more lipophilic dye conjugated to trastuzumab, **Trastu-($NMe_2$) AzaNIR II**, accumulated significantly more than the two other targeted-fluorophores in the tumor 6 days after injection ($p < 0.05$, Tukey multiple comparisons test), while there were no statistical differences at 48 h. Furthermore, tumor-to-muscle (from 6.2 to 23.7) and tumor-to-healthy ovary (from 2.3 to 7.6) ratios were calculated and confirmed these findings (Figure 7b,c). This latter result indicated a clear benefit in the contrast imaging as compared to non-coupled fluorophores.

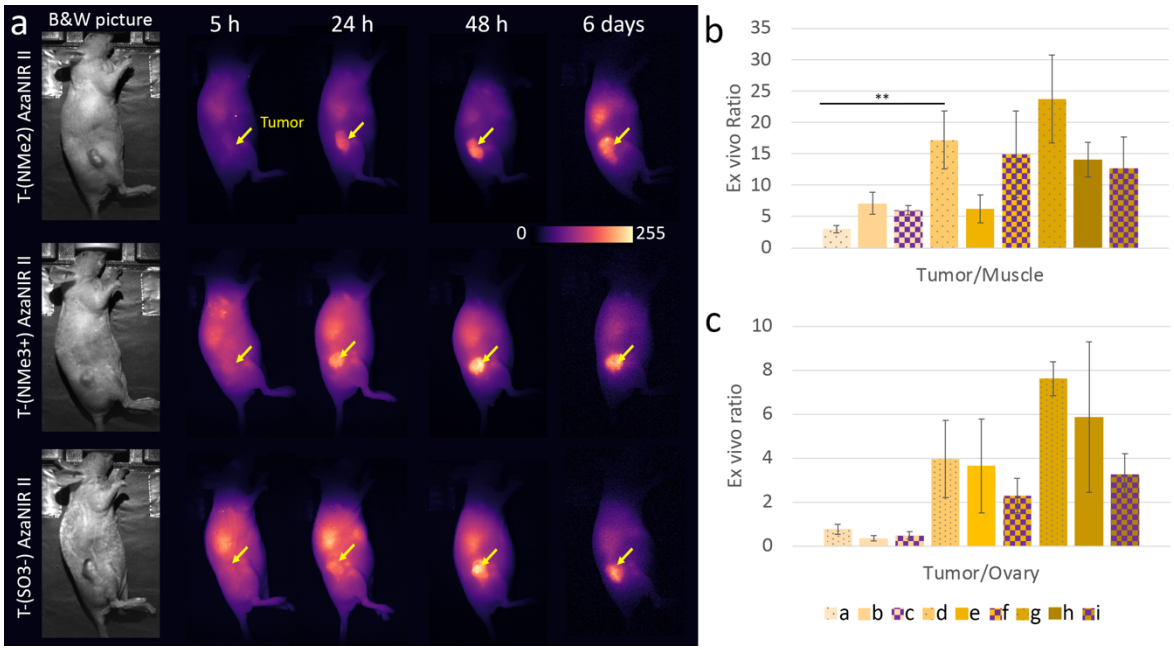


***Figure 7**: In vivo behavior of the different fluorophores coupled to trastuzumab. (a) Representative NIR-II images of mice bearing subcutaneous SKOV-3 tumors on their right flank at different times elapsed after administration of trastuzumab coupled fluorophores (i.e., 1.4 nmol of fluorophore). Color scale was standardized for all the captions. (b) Related tumor-to-muscle and (c) tumor-to-ovary ratios, from ex vivo quantification (Figure S17) and Figure 6 data. N = 3 / condition.** indicates a significant difference compared to ($NMe_2$) AzaNIR II compound alone and coupled to Trastuzumab, with p < 0.01. Color code: a, ($NMe_2$) AzaNIR II-48h; b, ($NMe_3^+$) AzaNIR II-48h; c, ($SO_3^-$) AzaNIR II-48h; d, Trastu($NMe_2$)*

*AzaNIR II-48h; e, Trastu($NMe_3^+$) AzaNIR II-48h; f, Trastu($SO_3^-$) AzaNIR II-48h; g, Trastu($NMe_2$) AzaNIR II-6 days; h, Trastu($NMe_3^+$) AzaNIR II-6 days; I, Trastu($SO_3^-$) AzaNIR II-6 days.*

When looking at the *in vitro* and *in vivo* results, it is really interesting to note that the more lipophilic **($NMe_2$) AzaNIR II** presented numerous advantages compared to the two other structures.

Injected alone, it accumulates less in the liver and the spleen than the other fluorophores. Even more interestingly, *in vivo*, the trastuzumab resulting bioconjugate shows better biodistribution and targeting properties than the other two bioconjugated. It was also interesting to note that, despite its slightly more pronounced lipophilic character, the molecule bioconjugates well *via* the transglutaminase pathway on trastuzumab.

This study has thus demonstrated that the presence of a charge on the second NMe2 group on the propargylamine of aza-BODIPYs certainly makes the molecules less lipophilic, but that this does not necessarily have a positive influence for biodistribution *in vivo*. These results point to the future development of aza-BODIPYs functionalized on one side by a functionalized propargylamine and on the other side by an uncharged group for future molecular imaging applications.

**CONCLUSION**

In conclusion, three new NIR II-emitting aza-BODIPYs were synthesized and studied. All three molecules have been successfully bioconjugated with trastuzumab via the transglutaminase methodology, and although the $NMe_2$ bioconjugate seems to aggregate more than the other two in PBS, biodistribution studies on mice bearing HER-2-positive tumors show a more favorable behavior for the more lipophilic molecule. While this study has demonstrated the influence of the different water-solubilizing groups at all levels, a comprehensive study is required to assess the potential of each fluorophore, particularly for aza-BODIPYs dyes. This work also paves the way for further optimization of NIR-II aza-BODIPY probes. Indeed, the addition of water-solubilizing group is not mandatory to achieve successful bioconjugation and can alter the overall fluorescence properties in biological medium. Nevertheless, a compromise needs always to be found between favorable photophysical characteristics and water-solubility, to allow at least the attachment on biological vectors such as antibodies without causing significant aggregation. Finally, beyond this project, the fine control of the desymmetrization of the propargylamine groups on the boron center opens the way to the easy construction of new dissymmetrical aza-BODIPYs systems, which represents a real advantage given the challenge of functionalizing these fluorophores in general.

**EXPERIMENTAL PART**

**Materials and methods**

**NMR Spectroscopy**: ($^{1}H$, $^{13}C$, $^{11}B$, $^{19}F$) were recorded at 298 K on Bruker spectrometers Avance Neo 500 MHz equipped with a 5 mm BBOF iProbe. NMR spectroscopy chemical shifts are quoted in parts per million (δ) relative to TMS (for $^{1}H$, $^{13}C$), $BF_3{*}Et_2O$ (for $^{11}B$), $CFCl_3$ ($^{19}F$), calibration was made by using residual signals of the partially deuterated solvent. For all other nuclei, SR value obtained after zero-calibration of the corresponding reference was applied.

**Mass Spectrometry**: High-resolution mass spectrometry analyses were recorded on a LTQ Orbitrap XL mass spectrometer (Thermo Scientific) equipped with an electrospray ionization source (HESI 2). The following source parameters were used if no further specification is mentioned: Heater Temperature: 50°C. Gas Flow: Sheath 15 / Aux 10 / Sweep 0 Spray Voltage: 4 kV Capillary Temperature: 275°C Capillary. Voltage: 22 V Resolution (m/z = 400): 60 000. Typical conditioning: A stock solution of the analyte was prepared by dissolving 1 mg of the analyte in 1 mL of a HPLC-grade solvent chosen from the following list: $CH_2Cl_2$, MeOH, $CH_3CN$, $H_2O$, or in RPE-grade DMSO. For small molecules (MW < 1000 Da) a 1/100 dilution was performed using 10.0 µL of the stock solution completed to 1.0 mL by a HPLC-grade solvent of the following list sorted by order of preference: MeOH, $H_2O$, $CH_3CN$, $CH_2Cl_2$. For high weight molecules (MW> 1000 Da) a 1/10 dilution was performed using 100.0 µL of the stock solution completed to 1.0 mL by a HPLC-grade solvent of the following list sorted by order of preference: MeOH, $H_2O$, $CH_3CN$, $CH_2Cl_2$. The $10^{-5}$ M resulting solution of the analyte was then directly infused into the spectrometer using a 500 µL syringe. The system was rinsed three times between two consecutive analyses with 500 µL of HPLC grade water and/or MeOH. Mass calibration in the 100-2000 Da mass range was operated using the commercially available Pierce LTQ ESI Positive/Negative ion Calibration solutions (Thermofisher Scientific ref 88322/88324).

NMR and mass-analyses were performed at the "Plateforme d'Analyse Chimique et de Synthèse Moléculaire de l'Université de Bourgogne" (PACSMUB).

**RP-HPLC-MS**: Analyses were performed on a ThermoFisher Vanquish instrument (pump + autosampler at 20 °C + column oven at 25 °C) equipped with a UV-visible DAD and ISQ-EM single quadrupole mass spectrometer. The chromatographic system detailed below was used for theses analyses. System: RP-HPLC-MS (Phenomenex Kinetex C18 column, 2.6 µm, 2.1 × 50 mm) with MeCN (+ 0.1% FA) and 0.1% aq. formic acid (aq. FA, pH 2.1) as eluents 5% to 100% (5 min) of B, then 100% B (3.0 min) at a flow rate of 0.5 mL/min or 5% to 100% (5 min) of B, then 100% B (5.0 min) at a flow rate of 0.5 mL/min for more hydrophobic compounds. UV-visible detection was achieved at 214, 254, 280 and 650 nm (+diode array detection in the range of 220-700 nm). Low resolution ESI-MS detection in the positive/negative mode

(full scan, 100-1000 a.m.u., spectrum type: centroid, dwell or scan time: 1 s, source CID voltage: 20 V, vaporizer temperature: 282°C, ion transfer tube temperature: 300 °C, source voltage positive ions: 3 kV, source voltage negative ions: -2 kV, sheet gas pressure: 49.9 psig (3.4 bars), aux gas pressure: 5.7 psig (0.35 bar) and sweep gas pressure: 0.5 psig (0.035 bar).

**Semi preparative chromatography**: Semi preparative separations were executed on a HPLC-system from Shimadzu that is equipped with 2 LC-20AT pumps, a SPD-20A UV/Vis detector, a FRC-10A fraction collector, a SIL-10AP sampler and a CBM-20A control unit. The column was a SiliCycle C18 10 µm 10x250 mm column. UV-visible detection was achieved at 220, 260, 600 and 700 nm. The gradients using a mixture of ACN and water with 0.1% FA with a flow rate of 20 mL/min are the following:

Gradient A :

| **Time [min]** | **% $H_2O$ + 0.1% formic acid** | **% ACN** |
|---|---|---|
| **0** | 90 | 10 |
| **2** | 90 | 10 |
| **5** | 80 | 20 |
| **65** | 20 | 80 |

Gradient B :

| **Time [min]** | **% $H_2O$ + 0.1% formic acid** | **% ACN** |
|---|---|---|
| **0** | 95 | 5 |
| **2** | 95 | 5 |
| **5** | 90 | 10 |
| **55** | 40 | 60 |

**Lyophilization**: Lyophilization operations were performed with a Christ Alpha 2-4 LD plus. The compounds were lyophilized during at least one night.

**Reagents and chemicals for synthesis**: Reactions were carried out in analytical reagent grade solvents from Carlo Erba under a normal atmosphere. Non-stabilized dry solvents were purchased from Carlo Erba and dried using a MB-SPS-800 (MBraun) or PureSolv-MD-5 (Inert). All reagents purchased from Sigma-Aldrich, Thermo Fisher Scientific, Broadpharm, New England Biolabs or Zedira were used as received without further purification. Reactions were monitored by thin-phase chromatography and

RP-HPLC−MS. Analytical thin-phase chromatography was performed using Merck 60 F254 silica gel (precoated sheets, 0.2 mm thick). Column chromatography was carried out using silica gel (SigmaAldrich; 40−63 µm 230−400 mesh 60 Å). Purity was determined from HPLC analysis and was >95% for all the injected compounds. Commercial solutions of trastuzumab (anti-HER2 antibody, Herceptin®) purchased from Roche were purified with a HiTrap™ Desalting column (GE Healthcare) and concentrated to 10 mg/mL in PBS.

## Synthesis

All the following reactions were monitored by RP HPLC MS:

**Compound 6**: Compound **5** (50 mg, 65 µmol, 1 eq) was dissolved in 10 mL of ACN. NaHCO3 (27 mg, 324 µmol, 5 eq) and propanesultone (6.8 µL, 77.9 µmol, 1.2 eq) were added. The reaction was refluxed overnight and the crude product was filtered to remove the excess of base, evaporated to dryness and purified by semi-preparative HPLC using gradient A, and lyophilized to isolate pure **6** as a blue powder (35 mg, 60% yield).**$^{1}$H NMR** (500 MHz, 298 K, MeOD) δ (ppm) 8.27 (d, $^{3}J$ = 8.9 Hz, 4H), 8.09 (d, $^{3}J$ = 8.9 Hz, 4H), 7.18 (d, $^{3}J$ = 8.9 Hz, 4H), 6.98 (s, 2H), 6.86 (d, $^{3}J$ = 8.9 Hz, 4H), 3.92 (s, 8H), 3.64 (s, 2H), 3.09 (s, 12H), 2.91 (t, $^{3}J$ = 6.8, 6.8 Hz, 2H), 2.79 (s, 6H), 2.66 (s, 6H), 2.12 (t, $^{3}J$ = 8.4 Hz, 2H).**$^{13}$C NMR** (125 MHz, DMSO-$d_6$) δ (ppm) 160.8, 156.1, 150.9, 141.99, 141.32, 132.0, 130.3, 124.2, 119.7, 115.9, 113.8, 111.9, 87.5, 86.1, 61.8, 55.5, 53.7, 49.4, 47.9, 46.8, 41.6, 18.6. **$^{11}$B NMR** (160 MHz, MeOD) δ (ppm) -13.13 (bs). **HR-MS** (ESI): m/z calculated for $C_{51}H_{58}BN_7O_5S$ $[M+H]^+$ 892.43860 Da, found 892.43803 Da. **Analytical HPLC**: $t_R$=4.50 min (Purity 98%).

Compound **($SO_3^-$) AzaNIR II**: Compound **6** (15 mg, 16.8 µmol, 1 eq) was dissolved in 5 mL of dry ACN. $NaHCO_3$ (7 mg, 84 µmol, 5 eq) and 202 µL of a solution of *N*-Boc-PEG4-bromide (20.2 mg, 50.5 µmol, 3 eq) in dry ACN at 100 mg/mL were added. The reaction was refluxed for 48 h. The crude product was filtered to remove the excess of base and evaporated to dryness. 1M HCl (5 mL) was added and the reaction was stirred at 40°C until complete hydrolysis (4h). Solvents were evaporated and the crude product was purified by semi-preparative HPLC using gradient B and lyophilized to isolate pure **($SO_3^-$)-AzaNIR II** as a blue powder (15 mg, 74% yield). **$^{1}$H NMR** (500 MHz, 298 K, DMSO-$d_6$) δ (ppm) 8.35 (d, $^{3}J$ = 9.0 Hz, 4H), 8.10 (d, $^{3}J$= 9.0 Hz, 4H), 7.78 (s, 2H), 7.29 (s, 2H), 7.23 (d, $^{3}J$ = 9.0 Hz, 4H), 6.86 (d, $^{3}J$ = 9.0 Hz, 4H), 4.09 (s, 2H), 3.92 (s, 2H), 3.90 (s, 6H), 3.78 – 3.71 (m, 2H), 3.39 – 3.32 (m, 2H), 3.53 – 3.44 (m, 12H), 3.39 – 3.32 (m, 4H), 3.07 (s, 12H), 3.00 – 2.91 (m, 2H), 2.89 (s, 6H), 2.69 (s, 6H), 2.57 (t, $^{3}J$ = 7.0 Hz, 2H), 1.98 (s, 2H).**$^{13}$C NMR** (125 MHz, DMSO-$d_6$) δ (ppm) 161.5, 156.2, 151.5, 142.4, 141.8, 132.7, 130.8, 124.5, 120.2, 116.4, 114.5, 112.5, 70.2, 70.1, 70.1, 70.02, 69.8, 69.5, 64.3, 62.5, 56.1, 55.9, 51.0, 50.01, 48.6, 40.6, 40.5, 40.4, 40.3, 40.2, 40.1, 40.09, 40.00, 39.9, 39.8, 39.6, 39.4, 19.3. **$^{11}$B NMR** (160

MHz, DMSO-$d_6$) δ (ppm) -12.56 (bs). **HR-MS** (ESI): m/z calculated for $C_{61}H_{80}BN_8O_9S$+ $[M]^+$ 1111.58565 Da; found 1111.58471 Da. **Analytical HPLC**: $t_R$ = 3.41 min (Purity 96%).

**Compound 7**: Compound **6** (75 mg, 97.4 µmol, 1 eq) was dissolved in 5 mL of dry ACN. $NaHCO_3$ (40.9 mg, 487 µmol, 5 eq) and 234 µL of a solution of N-Boc-PEG4-bromide at 100 mg/mL in dry ACN (46.8 mg, 117 µmol, 1.2 eq) were added. The reaction was refluxed overnight. The crude product was filtered to remove the excess of base and evaporated to dryness and was purified by semi-preparative HPLC using gradient A, and lyophilized to isolate pure **7** as a blue powder (30 mg, 27% yield). **$^1$H NMR** (500 MHz, 298 K, $CDCl_3$) δ 8.63 (ppm) (s, 1H), 8.21 (d, $^3J$ = 8.9 Hz, 4H), 8.03 (d, $^3J$ = 8.9 Hz, 4H), 6.98 (d, $^3J$ = 8.9 Hz, 4H), 6.76 (s, 2H), 6.75 (d, $^3J$ = 9.0 Hz, 4H), 3.88 (s, 6H), 3.66 (s, 2H), 3.64 – 3.60 (m, 2H), 3.55 – 3.46 (m, 12H), 3.43 (t, $^3J$ = 5.3 Hz, 2H), 3.29 – 3.24 (m, 4H), 3.22 (s, 2H), 3.06 (s, 12H), 2.79 (s, 6H), 2.21 (s, 6H), 1.40 (s, 9H).**$^{13}$C NMR** (125 MHz, $CDCl_3$) δ (ppm) 168.1, 160.9, 156.5, 156.1, 150.9, 143.0, 142.4, 132.1, 130.6, 125.5, 121.1, 115.7, 113.9, 113.4, 111.9, 93.6, 85.1, 79.1, 77.33, 77.28, 77.1, 76.8, 70.4, 70.3, 70.2, 70.1, 70.1, 70.0, 64.9, 62.3, 56.8, 55.8, 55.6, 50.9, 48.8, 44.0, 40.2, 29.7, 28.4.**$^{11}$B NMR** (160 MHz, $CDCl_3$) δ (ppm) -13.07 (bs). **HR-MS** (ESI): m/z calculated for m/z calculated for $C_{63}H_{82}BN_8O_8$+ $[M]^+$ 1089.63432 Da; found 1089.63359 Da. **Analytical HPLC**: $t_R$ = 3.940 min (Purity 100%).

**Compound ($NMe_2$) AzaNIR II**: Compound **7** (20 mg, 18.4 µmol) was solubilized in acetonitrile (5 mL) and HCl 1M (5 mL) was added. The reaction was stirred at 40°C until complete hydrolysis (4h). Solvents were evaporated and the crude product was purified by semi-preparative HPLC using gradient A, and lyophilized to isolate pure **($NMe_2$) AzaNIR II** as a dark blue powder (15 mg, 75% yield). **$^1$H NMR** (500 MHz, 298 K, $CDCl_3$) δ (ppm) 8.61 (s, 2H), 8.22 (d, $^3J$ = 9.0 Hz, 4H), 8.04 (d, $^3J$ = 9.0 Hz, 4H), 6.97 (d, $J$ = 9.0 Hz, 4H), 6.79 – 6.74 (m, 6H), 3.88 (s, 4H), 3.66 – 3.58 (m, 5H), 3.57 – 3.51 (m, 13H), 3.23 (s, 4H), 3.07 (s, 12H), 3.04 – 2.95 (m, 2H), 2.78 (s, 6H), 2.22 (s, 6H).**$^{13}$C NMR** (125 MHz, $CDCl_3$) δ (ppm) 167.3, 159.9, 155.5, 149.8, 142.0, 141.4, 131.1, 129.6, 124.6, 120.1, 114.7, 112.8, 112.4, 110.9, 92.6, 83.9, 76.3, 76.2, 76.0, 75.8, 69.3, 69.2, 69.2, 69.1, 68.9, 68.7, 67.6, 63.7, 61.2, 55.5, 54.6, 49.9, 47.8, 43.0, 39.2, 39.2, 38.7.**$^{11}$B NMR** (160 MHz, $CDCl_3$)) δ (ppm) -13.63 (bs). **HR-MS** (ESI): m/z calculated for $C_{58}H_{74}BN_8O_6$+ $[M]^+$ 989.58189 Da; found 989.58066 Da. **Analytical HPLC**: $t_R$ = 3.50 min (Purity 100%).

**Compound ($NMe_3^+$) AzaNIR II**: 20 mg (26 µmol) of **($NMe_2$) AzaNIR II** were dissolved in DCM (2 mL). 1 mL of MeI were added and the solution was stirred at room temperature for 15 min. The solution was evaporated to dryness and the residue was dissolved in ACN (3 mL). 3 mL of 1 M HCl were added and the reaction was stirred overnight at 40°C until complete deprotection (4h). Solvents were then evaporated and the crude product was purified by semi-preparative HPLC using gradient B, and

lyophilized to isolate pure **($NMe_3^+$) AzaNIR II** as a dark blue powder (15 mg, 67% yield).**$^1$H NMR** (500 MHz, 298 K, MeOD) δ (ppm) 8.55 (s, 2H), 8.27 (d, $^3J$ = 8.9 Hz, 4H), 8.11 (d, $^3J$ = 8.9 Hz, 4H), 7.12 (d, $^3J$ = 8.9 Hz, 4H), 7.05 (s, 2H), 6.85 (d, $^3J$ = 9.2 Hz, 4H), 4.06 (s, 2H), 3.97 (s, 2H), 3.91 (s, 6H), 3.75 – 3.68 (m, 2H), 3.57 – 3.47 (m, 14H), 3.30 – 3.24 (m, 2H), 3.10 (s, 12H), 2.96 (t, $^3J$ = 5.1 Hz, 2H), 2.90 (s, 6H), 2.86 (s, 9H).**$^{13}$C NMR** (125 MHz, MeOD) δ (ppm) 170.3, 162.9, 157.8, 152.9, 144.2, 144.0, 133.3, 131.8, 129.6, 126.4, 121.8, 116.7, 114.9, 113.1, 71.4, 71.4, 71.3, 71.2, 71.1, 68.9, 65.6, 63.9, 58.1, 57.5, 56.2, 52.9, 51.8, 49.5, 49.4, 49.3, 49.3, 49.2, 49.0, 48.8, 48.7, 48.5, 40.8, 40.4.**$^{11}$B NMR** (160 MHz, MeOD) δ (ppm) -12.90 (bs). **HR-MS** (ESI): m/z calculated for $C_{59}H_{77}BN_8O_6^{2+}$ $[M]^{2+}$ 502.30241 Th; found 502.30220 Da. **Analytical HPLC**: $t_R$=3.54 min (Purity 96%).

**Determination of logP**

An isocratic analysis (50 min) was performed by RP-HPLC (Thermo Hypersil GOLD C18 4.6 x 100 mm) using an eluent of 65% of [$H_2O$ /0.1 % FA] and 35% of [ACN /0.1 % FA]. The dead time was determined using formamide. The capacity factor (k) was calculated with the equation $k = (t_r-t_0) / t_0$, in which $t_r$ was the retention time and $t_0$ the dead time. Benzoic acid, toluene, bromobenzene, thymol and diphenylamine were used as standards. Mean values of three injections were used to calculate the resulting logP. The different HPLC analyses were performed at 25°C

The logP values were calculated with the equation $k = (t_R-t_0)/t_0$, where $t_0$ is the dead time (determined by injection of an unretained organic compound (formamide, $t_0$ = 1.23 min). Average values of three repeated injections.

**Photophysical characterizations**

Absorbance measurements were recorded on a UV-Vis-NIR spectrophotometer Cary5000 between 250 and 1100 nm. Steady-state photoluminescence spectra were measured from 700 to 1600 nm with a calibrated FSP 920 (Edinburgh Instruments, Edinburgh, United Kingdom) spectrofluorometer equipped with a nitrogen-cooled PMT R5509P. Relative measurements of photoluminescence QYs ($\Phi_{f,x}$) were performed using the dye IR125 dissolved in ethanol as reference. The QY of this dye was previously determined absolutely to $\Phi_{f,st}$ = 0.13. The relative QY were calculated according to the formula of Demas and Crosby, see equation below.

$$\Phi_{f,x} = \Phi_{f,st} \frac{F_x f_{st}(\lambda_{ex,st})}{F_{st} f_x(\lambda_{ex,x})} \frac{n_x^2(\lambda_{ex,x})}{n_{st}^2(\lambda_{ex,st})}$$

The subscripts x, st, and ex denote sample, standard, and excitation respectively. f(λ_ex) is the absorption factor, F the integrated spectral fluorescence photon flux, and n the refractive index of the

solvents used. All spectroscopic measurements were done in a 1 cm quartz cuvettes from Hellma GmbH at room temperature using air-saturated solutions.

**Bioconjugation studies**

**Deglycosylation of antibodies**: Antibody (2 mg/mL) in PBS pH 7.4 was incubated with 500 U/mg (one unit is defined as the amount of enzyme required to remove > 95% of the carbohydrate from 10 µg of denatured RNase B in 1 hour at 37°C in a total reaction volume of 10 µL) of protein of N-glycosidase F (PNGase F from NEB, New England Biolabs) overnight at 37 °C. The enzyme was then removed by centrifugation (Amicon Ultra-2 Centrifugal Filter Unit MWCO 50 kDa from Merck). The reaction was checked by LC-ESI-MS.

**Trastuzumab site-specific bioconjugation:** Deglycosylated trastuzumab (4 mg/mL) in PBS was incubated with 20 equivalents of the corresponding amine-functionalized NIRII probes (30 mM in DMSO) and with 3 U/mg of antibody of microbial transglutaminase (MTGase from Zedira). The resulting solution was stirred overnight (16 h) in a thermomixer (900 rpm) at 37 °C. The reaction was checked by LC-ESI-MS. Excess of substrate and MTGase were removed by FPLC purification. The recovered yield and masses of antibody engaged in the reaction are listed in the table bellowed with the corresponding DOL determined thanks to LC-ESI-MS analysis after purification.

**Fast protein liquid chromatography (FPLC) purification**: FPLC purification of the conjugates was performed on an ÄKTA™ 25 M system (GE Healthcare Life Sciences) with a Hitrap Mabselect™ column (MabSelect resin, Protein A, cross-linked agarose, column I.D. 7 mm, bed dimensions 7 x 25 mm, bed volume 1 mL). After deposition of the product, the conjugate was washed with 5 CV of PBS pH 7.4 (1 mL/min) followed by 5 CV of PBS 0.1 %Tween20 (1 mL/min) and 5 CV of PBS pH 7.4 (1 mL/min). Several washing cycles were performed until no free probes were detected. The conjugate was then eluted with 25 mM acetic acid (1 mL/min) and collected. Purification was monitored at 280 and 700 nm. Thereafter, the solution was transferred to an ultra-centrifugal filter device (Amicon Ultra 2 mL, Ultracel cut-off 30 kDa from Merck Millipore) and centrifuged at 4000 rpm for 3x15 min in order to condition the mixture in PBS (pH 7.4). Purification monitoring was performed using UNICORN™ 7.2 interface software (GE Healthcare).

**LC-ESI-MS**: Bioconjugation reactions were followed by reverse phase HPLC (Vanquish, Thermo Fisher Scientific) coupled to a high-resolution Orbitrap mass spectrometer (Exploris 240, Thermo Fisher Scientific) using an ESI source (positive mode). HPLC: A MabPac RP column (2.1 mm x 100 mm, 4µm,

Thermo Fisher Scientific) was used at 80°C (denaturing conditions), with a flow rate of 0.5 mL/min and a gradient 20-45% B in 6 min (eluents A: $H_2O$ + 0.02% TFA + 0.08% FA and B: ACN + 0.02% TFA + 0.08% FA). Mass: Full scan data were acquired at resolving power 30000 at m/z 200 in the m/z range 1000 – 4000. Data were analyzed with FreeStyle and BioPharma Finder 4.1 software (both Thermo Fisher Scientific). High-resolution mass spectra were deconvoluted using ReSpect function for intact antibody (150 kDa). Degree of labeling ratios were determined by comparison of native and conjugated antibody masses, using BioPharma Finder 4.1 software.

**Electrophoresis gel**: Each antibody sample was then diluted to 0.2 mg/mL in Laemmli buffer under either reducing (with 2-Mercaptoethanol and heating to 95°C for 5 minutes) to prepare them for separation by sodium dodecyl sulfate polyacrylamide gel electrophoresis (SDS-PAGE). For each experimental condition, 3 µg of antibody was deposited on the SDS-PAGE gel (4-20% acrylamide gel, Mini-PROTEAN TGX Stain-Free Gels) for 1.5 hours migration at 100 V. After migration, fluorescence analysis of the gel was performed on the ChemiDoc© MP imaging device (BioRad®) with an IRdye780 nm filter. Total protein revelation was achieved, thanks to stain-free imaging technology, on the ChemiDoc© MP imaging device (BioRad®) after an optimal exposure time for the stain-free gel activation. The protein ladder used was a PageRuler™ Prestained Protein Ladders, 10 to 180 kDa (Thermofisher Scientific).

**Biolayer Interferometry**: The HER-2 affinity of each conjugate was assessed by biolayer interferometry (BLI) on an Octet® R2 system (Sartorius). Biotinylated recombinant HER-2 protein (biotinylated Human Her2 / ErbB2 Protein, His Tag, ultra sensitivity, primary amine labelling, long spacer, Accrobiosystem®) were added on biosensors coated with a streptavidin layer (Octet® SA Biosensors, Sartorius). The loading of the biosensors was performed in wells containing biotinylated HER-2 protein concentrated to 20 nM in PBS during 300 s. The association phase was performed in wells containing different antibody concentrations in the range of 100 nM to 6.25 nM during 70 s. The dissociation phase was performed in PBS during 300 s. The experimental curves were aligned to the average last 5 s of the baseline, a Savitsky Golay filtering was applied and the curves were finally fitted with a 1:1 stoichiometry model using the Octet® Analysis Studio Software v12.2.2.26 in order to calculate the final $K_D$.

***In vitro* studies**

**Cell culture**: Human ovarian OVCAR-3 cells, (HER-2 negative) and human ovarian SKOV-3 cells (HER-2 positive) were obtained from the American Type Culture Collection (ATCC). OVCAR-3 cells were grown in RPMI medium supplemented with 10% fetal calf serum (FBS, Dutscher) and incubated in flasks at 37 °C, 5% $CO_2$ under humid atmosphere. Human ovarian SKOV-3 cells (HER-2 positive) were cultured similarly using Mc Coy enriched with 10% FBS. Cell lines were harvested and passaged when reaching 80% of confluence using trypsin.

**Microscopy**: HER2-positive SKOV-3 cells and HER2-negative OVCAR-3 cells (n = 50,000) were seeded on Lab-Tek chamber I, Nunc, 24 h before the experiment. Cells were incubated with 5 µg/mL of conjugated antibody and 1 µg/mL (in the presence of 0.01% DMSO) of non-coupled fluorophore in cell culture medium, for 60 min. The experiment was conducted at 4°C to observe the specific membrane targeting of the bioconjugated aza-BODIPYs, and possible passive uptake of the unconjugated molecules. The cells were then washed and counterstained with Hoechst 33342 (1 µM). Fluorescence microscopy images were acquired using a confocal laser-scanning microscope (LSM 710 Carl Zeiss, Jena, Germany) in APD live mode. Plan x63 objective was used (N. A. = 1.4 µm). Fluorescent signal was obtained with a 15% 633 nm excitation laser, and a collection wavelength > 650 nm. Images were processed using Fiji software. The experiments were performed at the MicroCell (Optical Microscopy-Cell Imaging, A. Grichine & M. Pyzet) platform, IAB Grenoble.

***In vivo* studies**

Animal experiments were performed in accordance with national legislation, and with the approval of the institutional and national (Ministère de l'Enseignement Supérieure et de la Recherche) animal ethics committees (APAFIS#8782), and were performed according to the Institutional Animal Care and Use Committee of Grenoble Alpes University and the Federation of European Animal Science Associations. These experiments were carried out within the small animal imaging platform Optimal (Dr V. Josserand), IAB Grenoble as described previously.[11] Briefly, female NMRI nude mice (6-week-old) (Janvier Labs, Le Genest-Saint Isle, France) were subcutaneously injected on their right flank with either 10 million of SKOV-3 cancer cells. Following tumor growth, mice were intravenously injected with either 200 µL of 200 µM fluorophores (i.e., <2% of DMSO) or 200 µL of 100 µg of conjugated antibody (i.e. 1.4 nmol of fluorophore, DOL = 2) solution diluted in PBS (n = 3 / condition). Whole-body NIR-II fluorescence imaging was performed before and at 5, 24, and 48 h after administration, on ventral, dorsal, and tumor sides (this latter is shown). For the antibody groups, a 6-day time-point was added. At the end of the imaging, the mice were euthanized and their organs were sampled for ex-vivo fluorescence imaging. Acquired images were analyzed using Fiji software. NIR-II fluorescence imaging

was performed using a Princeton camera 640ST (900–1700 nm) coupled to a laser excitation source of λ = 808 nm (50 mW/cm$^2$). A short-pass excitation filter at 1000 nm (Thorlabs), and a long-pass filter LP1064 nm (Semrock) were added to the NIR-II camera. A 25 mm lens with 1.4 aperture (Navitar) was used to focus on the mice.

**SUPPORTING INFORMATION AVAILABLE**

Detailed synthesis of intermediated compounds until compound **5**; characterization of the different compounds: NMR spectra, mass spectrometry, analytical HPLC; photophysical spectra of the different fluorophores in PBS; LC-ESI-MS and BLI sensorgram analysis for each bioconjugate; SEC analysis of each bioconjugate with their corresponding aggregation rate; flow cytometry and *in vivo* Tumor-to-Surrounding tissue ratios from animals. Molecular formula strings of the molecules.

**ASSOCIATED CONTENTS**

**AUTHOR INFORMATION**

**Corresponding authors**

**Christine Goze** - Institut de Chimie Moléculaire de l'Université de Bourgogne, ICMUB UMR CNRS 6302, Université de Bourgogne, Dijon 21000, France; Orcid https://orcid.org/0000-0002-3484-3837; Email: christine.goze@u-bourgogne.fr

**Catherine Paul** - Laboratoire d'Immunologie et Immunothérapie des Cancers, EPHE, PSL Research University, 75000 Paris; LIIC, EA7269, Université de Bourgogne, Dijon 21000, France; Orcid https://orcid.org/0000-0002-7657-5535; Email: catherine.paul@u-bourgogne.fr

**Lucie Sancey** - Université Grenoble Alpes, INSERM U 1209, CNRS UMR 5309, Institute for Advanced Biosciences, 38000 Grenoble, France; Orcid https://orcid.org/0000-0002-0084-3775; Email: lucie.sancey@univ-grenoble-alpes.fr

**Authors**

**Elisa Chazeau** - ICMUB, UMR 6302 CNRS, Université de Bourgogne, 9 av. A. Savary, BP 47870, 21078 Dijon, France; Laboratoire d'Immunologie et Immunothérapie des Cancers, EPHE, PSL Research University, 75000 Paris; LIIC, EA7269, Université de Bourgogne, 21000 Dijon, France.

**Christol Fabre** - Université Grenoble Alpes, INSERM U 1209, CNRS UMR 5309, Institute for Advanced Biosciences, 38000 Grenoble, France; Grenoble Alpes University Hospital, Grenoble, France.

**Malorie Privat** - ICMUB, UMR 6302 CNRS, Université de Bourgogne, 9 av. A. Savary, BP 47870, 21078 Dijon, France.

**Amélie Godard** - ICMUB, UMR 6302 CNRS, Université de Bourgogne, 9 av. A. Savary, BP 47870, 21078 Dijon, France.

**Cindy Racoeur** - Laboratoire d'Immunologie et Immunothérapie des Cancers, EPHE, PSL Research University, 75000 Paris; LIIC, EA7269, Université de Bourgogne, 21000 Dijon, France.

**Ewen Bodio** - ICMUB, UMR 6302 CNRS, Université de Bourgogne, 9 av. A. Savary, BP 47870, 21078 Dijon, France. Orcid https://orcid.org/0000-0003-2896-113X

**Benoit Busser** - Université Grenoble Alpes, INSERM U 1209, CNRS UMR 5309, Institute for Advanced Biosciences, 38000 Grenoble, France; Grenoble Alpes University Hospital, Grenoble, France; Institut Universitaire de France (IUF), Paris, France.

**Karl David Wegner** - Division Biophotonics, Federal Institute for Materials Research and Testing (BAM), 12489 Berlin, Germany. (https://orcid.org/0000-0003-0517-1880)

**Notes**

The authors declare no competing financial interest.

**ACKNOWLEDGMENTS**

The Ministère de l'Enseignement Supérieur et de la Recherche, the Centre National de la Recherche Scientifique (CNRS), the Conseil Régional de Bourgogne (PhD ICE grant 2021), and the French Research National Agency (ANR) *via* project JCJC "WAZABY" ANR-18-CE18-0012 are gratefully acknowledged. This work was also supported by grants from Ligue Contre le Cancer, Comité de Côte d'Or and Comité de l'Isère. The SATT Linksium supported AG. This work was performed within Pharm'image, a regional center of excellence in Pharmacoimaging, and the small animal imaging platform Optimal (Dr V. Josserand). Support was also provided by the French Government through the French National Research Agency (ANR) under the program "Investissements d'Avenir" (ANR-10-EQPX-05-01/IMAPPI

Equipex). M.-J. Penouilh and Q. Bonnin are gratefully acknowledged for HR-MS analyses. Finally, Pr. Anthony Romieu is warmly thanked for all his advances in photophysics.

**ABBREVIATIONS**

| | |
|---|---|
| Aza-BODIPY | aza-boron-dipyrromethene |
| BCN | bicyclo[6.1.0]non-4-yne |
| BLI | biolayer interferometry |
| Boc | tert-butyloxycarbonyl |
| BODIPY | Boro dipyrromethene |
| DBCO | dibenzocyclooctyne |
| DOL | degree of labeling |
| FBS | Foetal Bovine Serum |
| FGS | fluorescence-guided surgery |
| HER 2 | human epidermal growth factor receptor 2 |
| $K_D$ | affinity constant |
| IgG | Immunoglobulin G |
| mAb | monoclonal Antibody |
| MTGase | microbial transglutaminase |
| NIR | Near Infrared |
| PBS | phosphate buffer saline |
| PEG | polyethylene glycol |
| PNGASE F | Peptide -N-Glycosidase F |
| SDS-PAGE | sodium dodecyl sulfate polyacrylamide gel electrophoresis |
| SEC | size-exclusion chromatography |
| Wazaby | water-soluble aza-BODIPY |

## REFERENCES


[1] Pirovano, G., Roberts, S., Kossatz, S., Reiner, T. Optical Imaging Modalities: Principles and Applications in Preclinical Research and Clinical Settings. *J. Nucl. Med*. **2020**, *61(10)* ,1419-1427.

[2] Sutton P. A., van Dam, M. A., Cahill, R. A., Mieog, S., Polom, K., Vahrmeijer, A. L., ven der Vorst, J. Fluorescence-guided surgery: comprehensive review. *BJS Open*. **2023**, *7(3)*, zrad049.

[3] Li, J. B., Liu, H. W., Wang, R., Zhang, X. B., Tan, W. Recent Progress in Small-Molecule Near-IR Probes for Bioimaging. *Trends Chem*. 2019, *1(2)*, 224-234.

[4] Refaat, A., Yap, M.L., Pietersz, G. *et al.* In vivo fluorescence imaging: success in preclinical imaging paves the way for clinical applications. *J Nanobiotechnol.* **2022***, 20*, 450.

[5] Hong, G., Antaris, A., Dai, H. Near-infrared fluorophores for biomedical imaging. *Nat. Biomed. Eng.* **2017***, 1*, 0010.

[6] B., Zhao., L, Liao., Y, Zhu., Z, Hu., F, Wu. Near-infrared fluorescent Aza-BODIPY dyes: Rational structural design and biomedical imaging. *J. Lumin*. **2023**, *263*, 120099.

[7] Ilina, K., MacCuaig, W. M., Laramie, M., Jeouty, N., McNally, L.R., Henary, M. Squaraine Dyes: Molecular Design for Different Applications and Remaining Challenges. *Bioconjug Chem*. **2020**, *31(2)*, 194-213.

[8] Ge, Y., O'Shea, D. F. Azadipyrromethenes: from traditional dye chemistry to leading edge applications. *Chem. Soc. Rev.* **2016**, 45, 3846-64.

[9] Bodio, E., Goze, C. Development of BODIPYS and aza-BODIPYs for molecular imaging applications: From the in vitro to the in vivo, *AINC*, **2021**, *78*, 65-107.

[10] Lescure, R., Privat, M., Pliquett, J., Massot, A., Baffroy, O., Busser, B., Bellaye, P. S., Collin, B., Denat, F., Bettaïeb, A., Sancey, L., Paul, C., Goze, C., Bodio, E. Near-infrared emitting fluorescent homobimetallic gold(I) complexes displaying promising in vitro and in vivo therapeutic properties. *Eur. J. Med. Chem*. **2021**, *5*, 220:113483.

[11] Kamkaewa, A., Burgess, K. Aza-BODIPY dyes with enhanced hydrophilicity. *Chem. Commun.* **2015**, *51*, 10664-10667.

[12] Tasior,M., Murtagh, J., Frimannsson, D. O., McDonnella, S. O., O'Shea, D. F. Water-solubilised BF2-chelated tetraarylazadipyrromethenes. *Org. Biomol. Chem.* **2010**, *8*, 522-525.

[13] Niu, S.L., Ulrich, G., Ziessel, R., Kiss, A., Renard, P.Y., Romieu A. Water-soluble BODIPY derivatives. *Org. Lett*. **2009**, *11(10)*, 2049-2052.

[14] Niu, S.L., Massif, C., Ulrich, G., Ziessel, R., Renard, P.Y., Romieu, A. Water-solubilisation and bio-conjugation of a red-emitting BODIPY marker. *Org Biomol Chem*. **2011**, 66-69.

[15] Godard, A., Kalot, G., Pliquett, J., Busser, B., Le Guével, X., Wegner, K. D., Resch-Genger, U., Rousselin, Y., Coll, J.-L., Denat, F., Bodio, E., Goze, C., Sancey, L. Water-Soluble Aza-BODIPYs: Biocompatible Organic Dyes for High Contrast *In Vivo* NIR-II Imaging. *Bioconjugate Chem.* **2020**, *31*, 1088-1092.

[16] Godard, A., Kalot, G., Privat, M., Bendellaa, M., Busser, B., Wegner, K. D., Denat, F., Le Guével, X., Coll, J.-L., Paul, C., Bodio, E., Goze, C., Sancey, L. NIR-II Aza-BODIPY Dyes Bioconjugated to Monoclonal Antibody Trastuzumab for Selective Imaging of HER2-Positive Ovarian Cancer. *J. Med. Chem.* **2023**, *66*, 5185-5195.

[17] Chen, Y., Xue, L., Zhu, Q., Feng, Y., Mingfu, W. Recent Advances in Second Near-Infrared Region (NIR-II) Fluorophores and Biomedical Applications. *Front. Chem*. **2021**, *9*, 750404.

[18] Feng, X., Wei, L., Liu, Y., Chen, X., Tian, R. Orchestrated Strategies for Developing Fluorophores for NIR-II Imaging. *Adv. Healthcare Mater.* **2023**, 2300537.

[19] Lui, X., Yu, B., Shen, Y., Cong, H. Design of NIR-II high performance organic small molecule fluorescent probes and summary of their biomedical applications. *Coord. Chem. Rev*. **2022**, *468*, 214609.

[20] Yang, N., Song, S., Liu, C., Ren, J., Wang, X., Zhu, S., Yu, C. An aza-BODIPY-based NIR-II luminogen enables efficient phototheranostics. *Biomater. Sci*. **2022**, *10*, 4815-4821.

[21] Hu, Z., Fang, C., Li, B., Zhang, Z., Cao, C., Cai, M., Su, S., Sun, X., Shi, X., Li, C., Zhou, T., Zhang, Y., Chi, C., He, P., Xia, X., Chen, Y., Gambhir SS., Cheng Z., Tian J. First-in-human liver-tumour surgery guided by multispectral fluorescence imaging in the visible and near-infrared-I/II windows. *Nat. Biomed. Eng*. **2020**, *4(3)*, 259-271.

[22] Sato, K., Gorka, A.P., Nagaya, T., Michie, M.S., Nani, R.R., Nakamura, Y., Coble, V.L., Vasalatiy, O.V., Swenson, R.E., Choyke, P.L., Schnermann, M.J., Kobayashi, H. Role of Fluorophore Charge on the In Vivo Optical Imaging Properties of Near-Infrared Cyanine Dye/Monoclonal Antibody Conjugates. *Bioconjug. Chem*. **2016**, 404-413.

[23] Jeger, S., Zimmermann, K., Blanc, A., Grünberg, J., Honer, M., Hunziker, P., Struthers, H., Schibli, R. Site-specific and stoichiometric modification of antibodies by bacterial transglutaminase. *Angew. Chem. Int. Ed*. **2010**, *17(49*), 9995-9997.

[24] Dennler, P., Chiotellis, A., Fischer, E., Brégeon, D., Belmant, C., Gauthier, L., Lhospice, F., Romagne, F., Schibli, R. Transglutaminase-Based Chemo-Enzymatic Conjugation Approach Yields Homogeneous Antibody–Drug Conjugates. *Bioconjug Chem.* **2014**, *25 (3*), 569– 578.

[25] Romieu, A., Massif, C., Rihn, S., Ulrich, G., Ziessel, R., Renard, P.-Y. *New J. Chem*. **2013**, *37*, 1016-1027.

[26] Boswell, C. A., Mundo, E.E., Zhang, C., Bumbaca, D., Valle, N. R., Kozak, C. R., Fourie, A., Chuh, J., Koppada, N., Saad, O., Gill, H., Shen, B. Q., Rubinfeld, B., Tibbitts, J., Kaur, S., Theil, F. P., Fielder, P. J., Khawli, L. A., Lin, K. Impact of Drug Conjugation on Pharmacokinetics and Tissue Distribution of Anti-STEAP1 Antibody–Drug Conjugates in Rats. *Bioconjug Chem*. **2011**, *22(10)*, 1994–2004.

[27] Adumeau, P., Raavé, R., Boswinkel, M., Heskamp, S., Wessels, H.J.C.T., van Gool, A.J., Moreau, M., Bernhard, C., Da Costa, L., Goncalves, V., Denat, F. Site-Specific, Platform-Based Conjugation Strategy for the Synthesis of Dual-Labeled Immunoconjugates for Bimodal PET/NIRF Imaging of HER2-Positive Tumors. *Bioconjug Chem*. **2022** *33(3)*, 530-540.

[28] Privat, M., Bellaye, P. S., Chazeay, E., Racoeur, C., Adumeau, P., Vivier, D., Bernhard, C., Moreau, M., Collin, B., Bettaieb, A., Denat, F., Bodio, B., Paul, C., Goze, C. First Comparison Study of the In Vitro and In Vivo Properties of a Randomly and Site-Specifically Conjugated SPECT/NIRF Monomolecular Multimodal Imaging Probe (MOMIP) Based on an aza-BODIPY Fluorophore. *Bioconjugate Chem*. **2023,** *34(4)*, 621-628.

[29] Tumey, L. N. Antibody-Drug Conjugates: Methods and Protocols. *Methods Mol. Biol.* **2020**, *2078*, 1.

[30] Dennler, P., Chiotellis, A., Fischer, E., Brégeon, D., Belmant, C., Gauthier, L., Lhospice, F., Romagne, F., Schibli, R. Transglutaminase-Based Chemo-Enzymatic Conjugation Approach Yields Homogeneous Antibody–Drug Conjugates. *Bioconjugate Chem.* **2014**, *25(3)*, 569-578.

[31] Gundersen, M.T., Keillor, J.W., Pelletier, J. N. Microbial transglutaminase displays broad acyl-acceptor substrate specificity. *Appl Microbiol Biotechnol*. **2014**, *98*, 219-230.

[32] Wang, H., Liu, C., Han, J., Zhen, L., Zhang, T., He, X., Li, M. HER2 expression in renal cell carcinoma is rare and negatively correlated with that in normal renal tissue. *Oncology Letters*, **2012**, *4*, 194-198.

## Table of Contents graphic